Acoustic tomography for scalar and vector fields: theory and application to temperature and wind estimation

Ivana Jovanović,[a] Luciano Sbaiz, and Martin Vetterli[b]
Audiovisual Communications Laboratory, Ecole Polytechnique Fédérale de Lausanne (EPFL), 1015 Lausanne, Switzerland

Sound or acoustic tomography is a type of inverse problem. The idea of estimating physical quantities that influence sound propagation by measuring the parameters of sound propagation has proven to be successful in several practical domains, including medicine, seismology, oceanography. The use of acoustic tomography for estimating temperature and wind fields in the atmosphere has been shown to be possible as well and, moreover, its potentials have been demonstrated in field experiments. However, in most of the previous work, the algorithms used have not been proven to be the mathematically correct solution to the inverse problem.
This paper considers the problem of reconstructing 2D temperature and wind fields using acoustic tomography setups. Primarily, it is shown that the classical time-of-flight measurements are not sufficient for the reconstruction of wind fields. As a solution, an additional set of measurements is suggested. The proposed set is related solely to the parameters of sound propagation, namely to the angle-of-departure/arrival of sound waves, and together with the time-of-flights enables complete temperature and wind recovery in a general case. Special cases are also discussed, emphasizing the situations for which it is possible to reduce the required measurements to only one of the two proposed sets. Specifically, it is proven that when a temperature and a source-free 2D wind are observed on a bounded domain, the time-of-flight measurements are sufficient for the complete reconstruction. Conversely, the angle-of-departure/arrival measurements are sufficient to reconstruct a temperature and a curl-free 2D wind fields observed on bounded domains. Further, an iterative reconstruction algorithm that covers both the general and the special setups is proposed and possible variations to the main scheme are discussed. In order to evaluate the reconstruction a qualitative error analysis is given. Finally, the simulation results confirm the theoretical results and the iterative algorithm demonstrates fast convergence. Also, the simulation shows that the adopted bent ray model for sound propagation always outperform the straight ray model. The unknown temperature and wind fields are reconstructed with a high accuracy.

PACS numbers: 43.20.Dk, 43.28.Vd, 43.60.Rw
Keywords: Acoustic tomography, inverse problems, Helmholtz's decomposition, temperature, vector tomography, wind flow

I. INTRODUCTION

Tomography aims at recovering an unknown multi-dimensional field based on the interactions between the considered medium and the signals emitted by radiating devices and captured by appropriate sensors. For many decades, tomography methods have been widely used in physics, geophysics, medicine and technology for non-destructive testing. Examples include the use of magnetic resonance imaging to detect physiological alterations of living tissues, or seismic tomography to image the interior of the Earth. The success of the tomographic approach primarily stems from its noninvasive nature and the fact that a significantly larger amount of data can be obtained compared to the classical one-sensor one-measurement setup. Furthermore, it allows to acquire a global, as opposed to a punctual, knowledge of the measured field.

Acoustic tomography for monitoring phenomena in the atmosphere, particulary temperature and wind, was first proposed in the 1990's[1,2], as an attempt to use the techniques successfully applied in monitoring ocean's structure[3]. The application of acoustic tomography is enabled by the strong dependence of sound propagation on the spatial distribution of air temperature and wind flow. Moreover, the use of acoustic tomography for imaging these physical quantities in near ground atmosphere has been already demonstrated in field experiments[2,4,5]. However, in most of the previous work, the used algorithms have not been proven to be the mathematically correct solution to the inverse problem. Hence, the goal of this paper is to bring forth related material from adjacent fields of research, and to present some recent as well as new results. In particular, the questions of joint two-dimensional (2D) temperature and wind field reconstruction, for general and specific cases of wind field are settled.

A. 2D temperature and wind field estimation

The temperature estimation is known to be a *scalar* tomography problem in the sense that it amounts to recover a scalar function from its line-integrals by means of the Radon transform and its inversion. These integrals can be typically computed from the time taken by

[a] Electronic address: ivana.jovanovic@epfl.ch
[b] Also at Department of EECS, University of California at Berkeley, Berkeley, CA 94720.

a sound wave to propagate from a transmitter to a receiver, hereafter referred to as *time-of-flight*. The reconstruction of wind fields, however, deals with *vector* tomography, where the unknown field is described by a vector function. While time-of-flights are again sufficient to recover the complete wind field, the inverse problem that needs to be solved in this case is highly nonlinear, hence analytically intractable. Thus, it is then necessary to resort to linearization which, while being attractive from a computational standpoint, seriously limits the reconstruction ability. In fact, Johnson *et al.*[6] were the first to notice that linearizing the relationship between the time-of-flights and the wind field makes that one wind component becomes "invisible" to the reconstruction process. Later, Norton[7] laid the groundwork for a theoretical treatment of this problem by showing that, according to the Helmholtz theorem, every vector field can be written as the sum of an *irrotational* (or curl-free) and a *solenoidal* (or source-free) component, and that only the solenoidal part can be imaged from the time-of-flights. Additional measurements are thus required to reconstruct the missing component. It should be noted that this essential phenomena is often left out in the acoustic tomography literature. This has an unpredictable effect on the reconstruction and perpetuates the incorrect belief that the inverse problem is ill-conditioned while it is actually ill-posed.

In this paper, an additional set of acoustic measurements related to the angle-of-departure and the angle-of-arrival of the sound waves is suggested. An iterative algorithm that uses both the time-of-flight and the angle-of-departure/arrival measurements in order to recover the full temperature and wind field is proposed. Note that a related approach was suggested by Braun and Hauck[8] in the context of fluid tomography. They also proposed an additional set of measurements based on an optical Schlieren technique. However, their method is only applicable in rather specialized scenarios having an optical access, while our method uses only sound waves.

B. Bounded domains and special cases of wind field

In most physical setups we observe an unknown field on a bounded domain, where the boundary signifies the closed curve on which the transmitters and receivers reside. The reconstruction of source-free wind fields observed on a bounded domain is an important problem and here it is studied in more detail. The source-free condition is usually valid when considering a horizontal slice in the low boundary layer of the atmosphere since the vertical component of the wind is commonly neglected. Braun and Hauck[8] showed that bounded domains admit harmonic vector fields that are both irrotational and solenoidal and therefore the Helmholtz decomposition is not anymore unique. The commonly studied transform based solutions, i.e. the solution given by Radon or Fourier transform, fail to give the correct result as they separately reconstruct the solenoidal and the irrotational component, but it is not any longer clear what part of the solenoidal component is going to be reconstructed. To overcome this problem, Norton[7] proposed to measure the normal component of the field on the boundary, in addition to the time-of-flights.

Instead, we show that the time-of-flights are sufficient for the reconstruction of a source-free wind field on a bounded domain and no other measurements are needed. Moreover, the estimation of the wind field is reduced to the estimation of its solenoidal component and, consequently, the dimension of the problem is reduced to the half of the original one. We also design an algorithm that reconstruct the temperature and the source-free wind field from the time-of-flight measurements.

Another special cases of wind fields, as the 2D wind fields that are obtained as a slice of a 3D source-free wind, and irrotational wind fields, are also studied. It is shown what type of measurements are needed for their reconstruction.

C. Outline

This paper is organized as follows. Section II gives a brief introduction to the inverse problems, presents the theory of sound propagation, introduces the bent-ray model and shows the limitations of the time-of-flight measurements. It then emphasizes the importance of the Helmholtz's theorem and introduces an additional second type of measurements needed for temperature and full wind field reconstruction. A new method to obtain these measurements is also proposed. In Sec. III important practical scenarios are discussed, emphasizing the cases for which the required measurements can be reduced to only one of the two proposed sets. Section IV describes the algorithms needed for reconstruction of both general and special temperature and wind field cases. Section V analyzes the reconstruction error and gives the Cramer-Rao lower bound for time-of-flight estimation. The simulation results are shown in Sec. VI. Finally, in Sec. VII we give the concluding remarks.

D. A word on notation

In the sequel, the vectors and the matrices will be noted in bold, the average value of any parameter f will be noted as f_0, vector $\boldsymbol{s}$ will represent the unit vector tangent to the ray path Γ, and $\boldsymbol{s}_\perp$ will be the unit vector normal to $\boldsymbol{s}$, also $\boldsymbol{s}\,ds = d\boldsymbol{s}$ and $\boldsymbol{s}_\perp ds = d\boldsymbol{s}_\perp$. Scalar product of two vectors will be denoted with $\cdot$ and the vector product with $\times$.

II. THE INVERSE PROBLEM IN ACOUSTIC TOMOGRAPHY

A. General formulation

Acoustic tomography is a type of inverse problem: namely, the information brought by sound radiation through the field of interest is used to infer the local

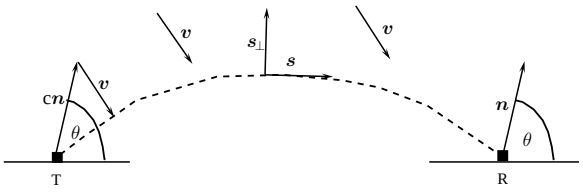

FIG. 1. Sound propagation. An example of a ray trajectory with the vectors $\boldsymbol{n}$, $\boldsymbol{s}$ and $\boldsymbol{s}_\perp$.

properties of the field. In the usual terminology of inverse problems[2], the set of parameters to be determined, which describes the state of the field, is called the model, $\mathcal{M}$. To obtain the information on the model parameters, measurements of some observable parameters are needed. The experimental measurements are called the data, $\mathcal{D}$. In order to compute the model parameters, first the forward problem is defined by devising a mapping $\mathcal{G}$ such that $\mathcal{D} = \mathcal{G}\mathcal{M}$. The inverse mapping $\mathcal{M} = \mathcal{G}^{-1}\mathcal{D}$ is then constructed from the forward mapping.

Usually solving a non-linear problem is analytically unsolvable and computationally intractable and thus forward problems are often *linearized*. Commonly, it is done by using the Taylor series expansion in terms of the models:

$$\mathcal{D} = \mathcal{G}\mathcal{M}_0 + \mathcal{G}_l(\mathcal{M} - \mathcal{M}_0) + \ldots,$$

and keeping only the first order terms, so that:

$$\mathcal{D} - \mathcal{D}_0 = \mathcal{G}_l(\mathcal{M} - \mathcal{M}_0), \tag{1}$$

where $\mathcal{G}_l$ is a linearized mapping around the unperturbated model $\mathcal{M}_0$. While inverse problems are often formulated in infinite dimensional spaces (or continuous domain), limitations to a finite number of measurements, and the practical consideration of recovering only a finite number of unknown parameters, usually lead to the problems being recast in discrete form. The discrete version of the problem is going to be discussed in the reconstruction algorithms while the continuous form appears to be very handy when showing the existence and uniqueness of the solution as well as other properties of interest.

In the rest of this section, our goal is to define a set of data acquired by acoustic tomography that enable wind and temperature reconstruction. The choice of course depends on the physics of sound propagation.

B. Sound propagation in the atmosphere and the influence of wind and temperature

The propagation of sound waves in an inhomogeneous moving medium, e.g. the atmosphere, is completely determined by the system of linearized equations of fluid dynamics[9]. When the medium inhomogeneities are large compared to the wavelength, the energy propagation is well described by the ray theory of sound propagation. The most simplified ray model is the straight-ray model, and it has been widely used in the previous research[10,11]. In this study a more accurate model is adopted, the so-called bent-ray model, that accounts for ray refraction.

The sound propagation is described by the group velocity and the vector $\boldsymbol{b}$ define in the following. The group velocity is

$$\frac{d\boldsymbol{x}}{dt} = c\boldsymbol{n} + \boldsymbol{v}, \tag{2}$$

where $\boldsymbol{x}$ is position, t is time, c is the sound speed, $\boldsymbol{n}$ is the unit vector normal to the wave front, and $\boldsymbol{v}$ is the wind velocity (see Fig. 1). The vector $\boldsymbol{b}$ is defined as $\boldsymbol{b} = \boldsymbol{k}/k_0$ with $\boldsymbol{k}$ being the wave vector and $\boldsymbol{b}$ has direction normal to the wave front, and

$$\frac{d\boldsymbol{b}}{dt} = -\frac{c_0\nabla c}{c} - \nabla(\boldsymbol{b}\cdot\boldsymbol{v}) + \frac{(\boldsymbol{b}\cdot\boldsymbol{v})\nabla c}{c}, \tag{3}$$

with ∇ being the gradient operator. The vector $\boldsymbol{b}$ is also normal to the wave front, i.e. $\boldsymbol{n} = \boldsymbol{b}/b$. From Eqs. (2) and (3) the ray path can be computed imposing some initial conditions for $\boldsymbol{x}$ and $\boldsymbol{b}$. For example, the starting point may correspond to the transmitter position $\boldsymbol{x}(0) = \boldsymbol{x}_T$, and the initial $\boldsymbol{b}(0)$ is chosen such that the ray reaches the receiver, while ensuring that in every point, $k + \boldsymbol{k}\cdot\boldsymbol{v}/c = k_0c_0/c$. Finally, taking into account Eqs. (2) and (3) and the fact that the sound speed is

$$c = 20.05\sqrt{T(1 + 0.511q)},$$

where T is the air temperature, and q is the mixing factor (usually between 0 and 0.03), it can be concluded that the sound propagation in the atmosphere strongly depends on temperature distribution and wind flow. In the following, we are going to see what are the observable parameters of the sound propagation that will enable the reconstruction of the temperature and wind field. In fact, since the temperature is uniquely determined from the sound speed, the aim will be to reconstruct c and $\boldsymbol{v}$.

C. Time-of-flight measurements and linearization

Time-of-flight measurements are the classical measurements provided by acoustic tomography methods. The time-of-flight from a transmitter to a receiver is equal to:

$$\tau = \int_\Gamma \frac{1}{(c\boldsymbol{n} + \boldsymbol{v})\cdot\boldsymbol{s}}\, ds, \tag{4}$$

where $\boldsymbol{s}$ is the unit vector tangent to the ray path Γ. Note that, the time-of-flight contains the information on c and $\boldsymbol{v}$ but it is rather impractical to choose Eq. (4) as the forward model. Instead, Eq. (4) is linearized as:

$$\begin{aligned}\tau &\simeq \int_\Gamma \frac{1}{c_0\boldsymbol{n}\cdot\boldsymbol{s}}\, ds - \int_\Gamma \frac{(\Delta c\boldsymbol{n} + \boldsymbol{v})\cdot\boldsymbol{s}}{(c_0\boldsymbol{n}\cdot\boldsymbol{s})^2}\, ds \\ &\simeq \tau_0 - \frac{1}{c_0^2}\int_\Gamma (\Delta c\boldsymbol{n} + \boldsymbol{v})\cdot d\boldsymbol{s},\end{aligned}$$

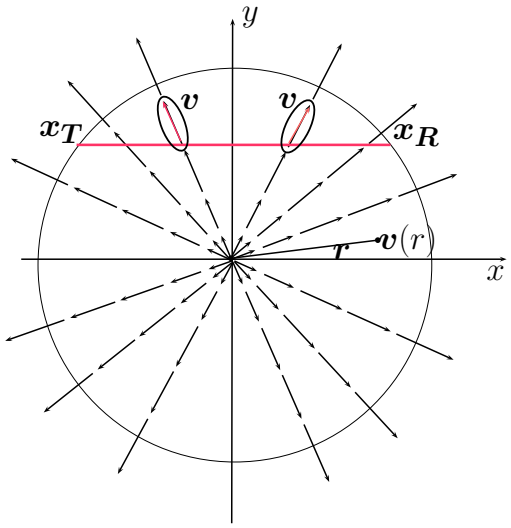

FIG. 2. One example of an "invisible" wind field. For any two points on the boundary $\boldsymbol{x}_T$ and $\boldsymbol{x}_R$ the longitudinal interactions sums up to zero.

where $\Delta c = c - c_0$, and Δc and $\|\boldsymbol{v}\|$ are typically much smaller than c_0. Now, the time-of-flight perturbations are linearly related to Δc and $\boldsymbol{v}$,

$$(\tau_0 - \tau)\, c_0^2 = \int_\Gamma (\Delta c \boldsymbol{n} + \boldsymbol{v}) \cdot d\boldsymbol{s}. \tag{5}$$

The line integral on the right hand side of Eq. (5) is also called the longitudinal interaction l_Γ by analogy with the line integrals of the vector field defined in Ref. 8,

$$l_\Gamma = \int_\Gamma (\Delta c \boldsymbol{n} + \boldsymbol{v}) \cdot d\boldsymbol{s}. \tag{6}$$

After all, it is important to check if from Eq. (6) we can uniquely determine the changes in c and $\boldsymbol{v}$, or equivalently if l_Γ is sufficient for estimating c and $\boldsymbol{v}$. The following example illustrates the answer.

Example 1 (Invisible wind): Assume a very particular synthetic wind field as shown in Fig. 2, i.e. $\boldsymbol{v}_1(\boldsymbol{r}) = \boldsymbol{r}$, as well as a particular measurement set up, i.e. the transmitters and the receivers are placed on a circle centered at the origin. For simplicity of exposure, the temperature is assumed to be constant, $\Delta c = 0$. Using the previously proposed linearization, the time-of-flights between any two points on the boundary ∂D are:

$$\tau \simeq \int_{-L}^{L} \frac{1}{c_0}\, ds - \frac{1}{c_0^2} \int_{-L}^{L} \boldsymbol{v}_1 \cdot d\boldsymbol{s} = \frac{2L}{c_0} = \tau_0$$

as the integral of an odd function over a symmetric interval is always equal to zero. As a result, the first order time-of-flight perturbations or equivalently the longitudinal interaction does not depend on this particular wind and hence no information on the field can be obtained whatsoever. Consequently, the time-of-flight perturbations τ_2 caused by any other wind field $\boldsymbol{v}_2$ would not differ from the perturbations caused by the wind $\boldsymbol{v}_1 + \boldsymbol{v}_2$ since $\boldsymbol{v}_1$ shows to be an "invisible" wind. Conversely, if we measure the time-of-flights τ_2 what is the underlying wind? Now it is clear that both $\boldsymbol{v}_2$ and $\boldsymbol{v}_2 + \boldsymbol{v}_1$ are the correct answers and therefore we need more information to resolve this ambiguity. Again, the non-linear model provides more information since

$$\begin{aligned}\tau &= \int_{-L}^{L} \frac{1}{c_0 + \boldsymbol{v}_1 \cdot \boldsymbol{s}}\, ds = \int_{-L}^{L} \frac{1}{c_0 + s}\, ds \\ &= \log(c_0 + L) - \log(c_0 - L) \neq \tau_0,\end{aligned}$$

but it is of little practical interest, due to the difficulty in solving a non-linear inverse problem. □

D. Scalar and vector tomography

There are two main classes of problems that appear in tomography. Namely, in the classical tomography problem, often referred as *scalar tomography*, it is assumed that every point of the unknown field is characterized by a scalar. Mathematically, this problem is equivalent to the problem of recovering a scalar function when knowing the values of its line integrals. The solution is found by applying the inverse Radon transform. A different type of problem appears when the unknown field is a vector field. In this class of the so-called *vector tomography* problems every component of the field is represented by an independent scalar function. However, it is not true anymore that the vector function can be recovered from the values of its line integrals. The latter become obvious if we consider the Helmholtz's decomposition of vector fields.

Recall that according to the Helmholtz's theorem, every vector field can be decomposed into an irrotational $\boldsymbol{v}_I$ (or curl-free, $\boldsymbol{\nabla} \times \boldsymbol{v}_I = 0$) and solenoidal $\boldsymbol{v}_S$ (or source-free, $\boldsymbol{\nabla} \cdot \boldsymbol{v}_S = 0$) component:

$$\boldsymbol{v}(\boldsymbol{x}) = \boldsymbol{v}_I(\boldsymbol{x}) + \boldsymbol{v}_S(\boldsymbol{x}).$$

The decomposition is not unique, since there exist fields which can be both curl-free and source-free, and they are called harmonic fields. For example, in a bounded domain D, the harmonic fields are the special cases of curl-free fields having the sources outside the domain D, or the source-free fields whose curls are closing outside the domain D. Sometimes, it is appropriate to separate this third harmonic component and to make the decomposition unique, but for now we will keep the two component representation. The two components can be described using potential functions:

$$\begin{aligned}\boldsymbol{v}_I(\boldsymbol{x}) &= \boldsymbol{\nabla} \phi(\boldsymbol{x}) \\ \boldsymbol{v}_S(\boldsymbol{x}) &= \boldsymbol{\nabla} \times \boldsymbol{\psi}(\boldsymbol{x}),\end{aligned}$$

where ϕ and $\boldsymbol{\psi}$ are the scalar and vectorial potentials of the field $\boldsymbol{v}$. For a two-dimensional field, e.g. in the xy-plane, $\boldsymbol{\psi}$ has only a component along the z axis: $\boldsymbol{\psi} =$

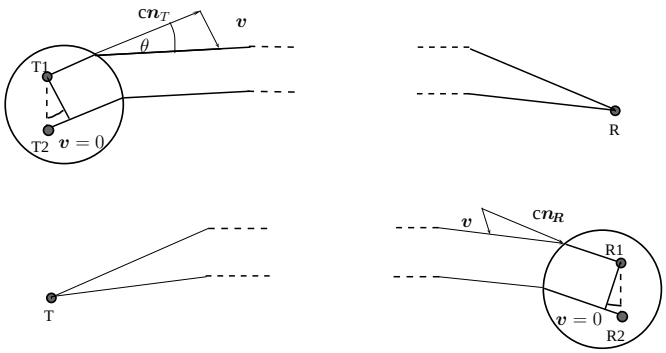

FIG. 3. The vector $\boldsymbol{n}_T$ and $\boldsymbol{n}_R$ can be estimated by measuring the angle-of-departure and the angle-of-arrival of the sound wave when $\boldsymbol{v}=0$ at the measuring point.

$\psi\,\boldsymbol{e}_z$. The representation using potentials is equivalent to the full knowledge of the vector field and it amounts to represent a vector field with the two scalar functions $\phi(\boldsymbol{x})$ and $\psi(\boldsymbol{x})$. Applying the Helmholtz's decomposition on $\boldsymbol{v}$ in Eq. (6), and assuming for simplicity that $\Delta c = 0$, we have

$$\begin{aligned} l_\Gamma &= \int_\Gamma (\nabla\phi + \nabla\times\boldsymbol{\psi})\cdot d\boldsymbol{s} \\ &= \phi(\boldsymbol{x}_R) - \phi(\boldsymbol{x}_T) + \int_\Gamma \frac{\partial\psi}{\partial y}s_x - \frac{\partial\psi}{\partial x}s_y\, ds, \end{aligned}$$

where the latter equality comes from the gradient theorem, i.e. $\int_a^b \nabla f\cdot d\boldsymbol{s} = f(b) - f(a)$. Notice that, except for the boundary values, the longitudinal interaction does not give any information on the irrotational wind component.

E. Additional set of measurements for irrotational wind component

In the past, several researches working in the field of fluid tomography came to the conclusion that the time-of-flight measurements are not sufficient for the vector field reconstruction[6–8]. In Ref. 8, the authors proposed a new set of measurements called the *transversal* interaction, which together with the longitudinal interaction allow to recover both the solenoidal and the irrotational components of a vector field. The transversal interaction corresponds to the integration of the normal component of the vector field along the propagation path

$$t_\Gamma = \int_\Gamma \boldsymbol{v}\cdot d\boldsymbol{s}_\perp,$$

and it provides the information on the irrotational component of the vector field since

$$\begin{aligned} t_\Gamma &= \int_\Gamma (\nabla\phi + \nabla\times\boldsymbol{\psi})\cdot d\boldsymbol{s}_\perp \\ &= -\psi(\boldsymbol{x}_R) + \psi(\boldsymbol{x}_T) + \int_\Gamma \frac{\partial\phi}{\partial y}s_x - \frac{\partial\phi}{\partial x}s_y\, ds. \end{aligned}$$

To obtain the transversal interaction, the authors in Ref. 8 suggest an optical Schlieren technique that is only practical in rather specialized setups having an optical access. We suggest a new method for estimating the transversal interaction based solely on the acoustic measurements.

Let us first slightly modify the definition of the transversal component so that it takes into account the temperature fields as well:

$$t_\Gamma = \int_\Gamma (\Delta c\boldsymbol{n} + \boldsymbol{v})\cdot d\boldsymbol{s}_\perp.$$

Notice that the group velocity along the trajectory is tangent to the trajectory, hence in every point

$$(c_0\boldsymbol{n} + \Delta c\boldsymbol{n} + \boldsymbol{v})\cdot \boldsymbol{s}_\perp = 0.$$

The transversal component can thus be written as

$$t_\Gamma = -c_0\int_\Gamma \boldsymbol{n}\cdot d\boldsymbol{s}_\perp.$$

In order to estimate t_Γ we need to know $\boldsymbol{n} = (\cos\theta\ \ \sin\theta)^T$, see Fig. 1, along the trajectory Γ. In a first approximation, it can be supposed that $\boldsymbol{n}$ is constant along Γ which is true when the temperature and wind fields are uniform[12]. Then

$$\begin{aligned} t_\Gamma &= c_0\int_\Gamma \begin{pmatrix}\cos\theta\\ \sin\theta\end{pmatrix}\cdot(\boldsymbol{s}\times\boldsymbol{e}_z)\, ds \\ &\simeq c_0\left(\cos\theta(y_R - y_T) - \sin\theta(x_R - x_T)\right), \end{aligned} \tag{7}$$

where $\boldsymbol{s}_\perp = -\boldsymbol{s}\times\boldsymbol{e}_z$, and t_Γ can be approximately computed if we know the angle θ and the exact position of the transmitter and the receiver. A better approximation of t_Γ can be obtained if $\theta = (\theta_T + \theta_R)/2$ where θ_T and θ_R are the corresponding angles at the transmitter and the receiver side respectively. Also, an improvement can be achieved if we assume that Γ is known (from the previous iteration) and the vector $\boldsymbol{n}$ changes linearly from $\boldsymbol{n}_T$ at the transmitter side to $\boldsymbol{n}_R$ at the receiver side. The angles θ_T and θ_R can be measured and they are actually equivalent to the angle-of-departure and the angle-of-arrival respectively of the sound wave when $\boldsymbol{v}=0$ at the measuring point. The condition $\boldsymbol{v}=0$ can be insured by using the wind shields as show in Fig. 3. The angle-of-departure/arrival can be measured using an acoustic dipole or a directional microphone like the *Blumlein* microphone. More practical details on how to measure θ are left for the appendix (see Appendix).

F. Correct definition of the inverse problem

Finally, the transversal and the longitudinal interactions together uniquely determine the temperature and the wind field and they both can be estimated by measuring the parameters of sound propagation. The correct general formulation of the forward problem is then

$$l_\Gamma = \int_\Gamma (\Delta c\boldsymbol{n} + \boldsymbol{v})\cdot d\boldsymbol{s} \tag{8a}$$

$$t_\Gamma = \int_\Gamma (\Delta c \boldsymbol{n} + \boldsymbol{v}) \cdot d\boldsymbol{s}_\perp. \tag{8b}$$

In the following, important practical scenarios will be discussed emphasizing the situations in which the set of measurements can be reduced to either Eq. (8a) or Eq. (8b). Before we continue, note that when $\boldsymbol{v} = 0$ the temperature estimation can be obtained from any of the two Eqs. (8), and actually the problem reduces to a scalar tomography problem.

III. SPECIAL PRACTICAL CASES

There are important practical scenarios that deserve to be studied in more detail. They are all related to the special cases of wind field since the temperature estimation was shown to be an "easy" problem. Also, they all consider the fields on a bounded region, where in practical setups the boundary refers to the closed curve on which the sources and receivers reside.

A. 2D projection of a 3D source-free wind field

A usual situation in practice is that the 2D wind field to be reconstructed is obtained by taking out a slice from a 3D source-free wind field, as the latter is a common case in the atmosphere. However, since the flow leaves and enters the slice, the assumption of the absence of the sources is not valid anymore. Indeed, it is easy to see that the source-free condition for a 3D wind field, $\nabla \cdot \boldsymbol{v} = 0$, in general does not extend to any of its 2D slices, for example in the xy-plane we have

$$\nabla \cdot \boldsymbol{v}_{xy} = \frac{\partial v_x}{\partial x} + \frac{\partial v_y}{\partial y} = -\frac{\partial v_z}{\partial z} \neq 0. \tag{9}$$

It should be then concluded that in this case both l_Γ and t_Γ are needed for the reconstruction and no simplification can be made.

B. Source-free 2D wind field: Horizontal slice in the stratified atmosphere

In the atmosphere there is a usual stratification cased by gravity. Since the horizontal component $\boldsymbol{v}_{xy}$ is as a rule greater than the vertical component v_z by factor of $10 - 100$, it can be often assumed that $v_z = 0$. Hence, by inserting this assumption into Eq. (9) the source-free condition in the horizontal plane will now be satisfied, i.e. $\nabla \cdot \boldsymbol{v}_{xy} = 0$ and the wind field $\boldsymbol{v}_{xy}$ can be approximated to the solenoidal field.

We have seen that the longitudinal interaction contains the information on the solenoidal wind field and the problem seems to be solved. However, recall that bounded domains admit harmonic fields that can be seen both as solenoidal or irrotational. Nevertheless, the transform based solutions usually reconstruct separately the solenoidal and the irrotational part of the field but it is not any longer clear what part of the solenoidal component is going to be reconstructed. For example, the authors in Ref. 8 propose to decompose the solenoidal field into the "pure" solenoidal homogeneous component $\boldsymbol{v}_{S_0}$ and the residual harmonic component $\boldsymbol{v}_H$,

$$\boldsymbol{v} = \boldsymbol{v}_S = \boldsymbol{v}_{S_0} + \boldsymbol{v}_H,$$

where $\boldsymbol{v}_{S_0}$ is homogeneous in that its normal component is zero on the boundary (completely tangential). In their solution, derived from the original inverse Radon's transform, it is shown that in the case of a circular geometry setup the obtained result consists of $\boldsymbol{v}_{S_0}$ and only one-half of $\boldsymbol{v}_H$. The problem that the harmonic field is reconstructed with only one half of its magnitude can be further treated by reapplying the same inversion in order to achieve the correct reconstruction. However, the harmonic component will be imagined differently in different geometry setups and the successful reconstruction might not be always possible. Another more general approach was suggested by Norton in Ref. 7, where he showed that the measurements of the normal component of $\boldsymbol{v}$ taken on the boundary ∂D can be used to resolve the ambiguity of the harmonic part.

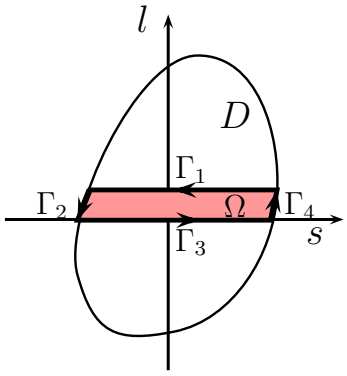

FIG. 4. Source-free vector field in a bounded domain D is uniquely determined from its line integrals taken over D.

Here, we want to show that no additional measurements are required in order to determine the source-free wind field on the bounded domain. Towards this end, it suffices to prove that the time-of-flights (in terms of the line-integrals) uniquely represent the field. This result is stated in the following theorem.

Theorem 1 *The source-free vector field $\boldsymbol{v}$ in a bounded simply connected domain D is uniquely determined from the longitudinal interaction through D.*

Proof 1 *Assume that there exist two different source-free vector fields $\boldsymbol{v}$ and $\boldsymbol{u}$ with the same line integrals through D,*

$$\int_\Gamma \boldsymbol{v} \cdot d\boldsymbol{s} = \int_\Gamma \boldsymbol{u} \cdot d\boldsymbol{s}, \quad \text{for all } \Gamma \text{ in } D.$$

Applying the 2D version of the Stoke's theorem on the difference field $(\boldsymbol{v} - \boldsymbol{u})$ and taking $\Gamma = \partial\Omega$ for any $\Omega \in D$

we have

$$\oint_{\partial\Omega} (\boldsymbol{v}-\boldsymbol{u})\cdot d\boldsymbol{s} = \iint_{\Omega} \boldsymbol{\nabla}\times(\boldsymbol{v}-\boldsymbol{u})\cdot \boldsymbol{e}_z \, ds\, dl$$
$$\oint_{\partial\Omega} \boldsymbol{v}\cdot d\boldsymbol{s} - \oint_{\partial\Omega} \boldsymbol{u}\cdot d\boldsymbol{s} = \iint_{\Omega} \boldsymbol{\nabla}\times(\boldsymbol{v}-\boldsymbol{u})\cdot \boldsymbol{e}_z \, ds\, dl. \quad (10)$$

The left hand side of Eq. (10) is identically equal to zero, since the corresponding line integrals along each of Γ_1, Γ_2, Γ_3 *and* Γ_4 *(see Fig. 4) are equal. Taking the derivative over* l*, we get*

$$0 = \int_{\Gamma_1} \boldsymbol{\nabla}\times(\boldsymbol{v}-\boldsymbol{u})\cdot \boldsymbol{e}_z \, ds. \quad (11)$$

In the previous equation, $\boldsymbol{\nabla}\times(\boldsymbol{v}-\boldsymbol{u})\cdot\boldsymbol{e}_z$ *is a scalar value and does not depend on the mutual orientation of* Γ *and* $\boldsymbol{v}-\boldsymbol{u}$*. Therefore, Eq. (11) coincides with the Radon transform of this value and since it is always zero we can conclude that the value itself is identical to zero almost everywhere,*

$$\boldsymbol{\nabla}\times(\boldsymbol{v}-\boldsymbol{u}) = 0.$$

Hence,

$$\boldsymbol{v}-\boldsymbol{u} = \nabla\varphi$$

almost everywhere, for some potential function φ *defined on* D*. Then, it also holds that*

$$0 = \int_{\Gamma} (\boldsymbol{v}-\boldsymbol{u})\cdot d\boldsymbol{s} = \int_{\Gamma} \nabla\varphi\cdot d\boldsymbol{s} = \varphi(\boldsymbol{x}_R) - \varphi(\boldsymbol{x}_T).$$

Here, Γ *is arbitrary, which leads to the conclusion that*

$$\varphi = const. \quad on\ \partial D.$$

Also, the field $\nabla\varphi$ *is by construction irrotational and since it represents the difference of the two solenoidal fields, it is also solenoidal. These two conditions are satisfied only when the field is a harmonic field. The harmonic fields on* D*, satisfies the solutions of the Laplace equation, and they are uniquely determined by its boundary values. Therefore,*

$$\varphi = const. \quad on\ D,$$

and then

$$\nabla\varphi = 0 \quad on\ D,$$

proves that $\boldsymbol{v}=\boldsymbol{u}$*, and the source-free field* $\boldsymbol{v}$ *is uniquely determined from its line integrals.* □

The above theorem demonstrates that the line integrals contain sufficient information for the reconstruction of source-free vector fields. Although, we show that the transform is injective and therefore, the inverse transform exists, we do not provide the explicit inversion formula. Instead, we are going to use algebraic reconstruction methods to reconstruct the unknown field. These methods are discussed in Sec. IV.

C. Reconstruction of the irrotational wind fields on bounded domains

It is possible to draw an analogy between the previous case and the case of irrotational wind fields.

Theorem 2 *The curl-free vector field* $\boldsymbol{v}$ *in a bounded simply connected domain* D *is uniquely determined from the transversal interaction* t_Γ *through* D*.*

Proof 2 *Assume also that there exist two different curl-free vector fields* $\boldsymbol{v}$ *and* $\boldsymbol{u}$ *with the same* t_Γ *integrals through* D*,*

$$\int_{\Gamma} \boldsymbol{v}\cdot d\boldsymbol{s}_\perp = \int_{\Gamma} \boldsymbol{u}\cdot d\boldsymbol{s}_\perp, \quad for\ all\ \Gamma\ in\ D.$$

Because the fields are irrotational, we have:

$$\boldsymbol{v} = \nabla\phi_1,$$

$$\boldsymbol{u} = \nabla\phi_2,$$

and the transversal interaction can be rewritten as:

$$\int_{\Gamma} \boldsymbol{v}\cdot d\boldsymbol{s}_\perp = \int_{\Gamma} \nabla\times\phi_1\boldsymbol{e}_z\cdot d\boldsymbol{s} = \int_{\Gamma} \boldsymbol{v}'\cdot d\boldsymbol{s}$$
$$\int_{\Gamma} \boldsymbol{u}\cdot d\boldsymbol{s}_\perp = \int_{\Gamma} \nabla\times\phi_2\boldsymbol{e}_z\cdot d\boldsymbol{s} = \int_{\Gamma} \boldsymbol{u}'\cdot d\boldsymbol{s}.$$

It then also holds that

$$\int_{\Gamma} \boldsymbol{v}'\cdot d\boldsymbol{s} = \int_{\Gamma} \boldsymbol{u}'\cdot d\boldsymbol{s} \quad for\ all\ \Gamma\ in\ D.$$

Applying the results from Theorem 1, we have $\boldsymbol{v}' = \boldsymbol{u}'$ *and*

$$\nabla\times\phi_1\boldsymbol{e}_z = \nabla\times\phi_2\boldsymbol{e}_z.$$

From the previous equation it also holds that

$$\nabla\phi_1 = \nabla\phi_2 \quad \Rightarrow \boldsymbol{v} = \boldsymbol{u}.$$

□

The theorem proves that the transversal interaction uniquely determines an irrotational wind field on a bounded region and it can be useful in case we are specifically interested only in the irrotational wind component.

IV. RECONSTRUCTION ALGORITHMS

So far, we have used continuous transforms, e.g. Radon transform, on which we can then choose to apply continuous inversions, e.g. inverse Radon transform, Fourier slice theorem, back projection etc. However, the Radon transform assume the knowledge of the line integrals of the unknown function for all the lines and all the directions. Even its discrete version requires a large number of projections with a special geometric setup, for example, the projections have to be uniformly distributed over

180° or 360°, in order to produce the results with a reasonable accuracy. An entirely different approach for tomographic reconstruction consists of first assuming that the measured field can be represented by an array of $\mathcal{M}$ parameters $m_1, m_2, \ldots, m_M$, and then setting up a linear set of equations for the unknowns in terms of $\mathcal{D}$, i.e. the measured data $d_1, d_2, \ldots, d_N$. This allows the forward problem in Eq. (1) to be written in the following matrix form:

$$\boldsymbol{d} = \boldsymbol{G}\boldsymbol{m}, \tag{12}$$

where $\boldsymbol{d}$ and $\boldsymbol{m}$ are column vectors whose elements are $d_i - d_{0i}$ and $m_i - m_{0i}$, and $\boldsymbol{G}$ is an $N \times M$ matrix whose elements are

$$G_{ij} = \frac{\partial d_i}{\partial m_j}.$$

Actually, Eq. (12) should represent the discretized version of Eqs. (8).

A. Linear vs. non-linear tomography algorithm

In the context of Eq. (12) we can define two problems. In *linear tomography*, we are given $\boldsymbol{G}$ and $\boldsymbol{d}$, and the objective is to determine $\boldsymbol{m}$. The assumption here is that the ray paths are known *a priori*. Typically, they are assumed to be straight lines. In *non-linear tomography*, we are given only the observation $\boldsymbol{d}$, and the goal is to infer $\boldsymbol{m}$ and incidently $\boldsymbol{G}$. In this case, the ray paths are not known and the dependence between the paths and the unknown fields is acknowledged. In non-linear tomography, an iterative algorithm[12] is needed to find the solution. The iterations alternate between estimating the temperature and the wind field and computing the trajectories. The basic structure of such an algorithm is given in Algorithm 1.

Analyzing the algorithm we see that there are only two significant calculations contained in it. *Step 2* is just the solution of the forward problem and it should not introduce any instability, since it can be performed essentially as accurately as the computing budget permits. *Step 4* on the other hand is crucial for the stability of the algorithm and it is actually the main step both in the linear and non-linear tomography. The desired solution to the inverse problem will not in general be the simple matrix inversion because either: 1) not all of the data are linearly independent, and/or 2) not all of the models are linearly independent. The latter indicates that there are multiple solutions to the same data set and the results of the theoretical analysis carried in the previous section should be used to choose the proper data sets and the proper model to avoid this case. Additionally, the matrix $\boldsymbol{G}$ might be poorly conditioned, and the noisy data may prevent from finding the exact solution to the system in Eq. (12). There is a vast area of the inverse methods trying to deal with all these problems. Unfortunately a detailed analysis is beyond the scope of this paper and it is to be treated elsewhere. Still, a brief classification might be of help.

B. Inverse methods overview

Group 1: A common idea behind most of the inversion methods is to minimize the error $\boldsymbol{e} = \boldsymbol{d} - \boldsymbol{G}\boldsymbol{m}$ in some sense. The error l_2-norm minimization is achieved in the methods like the Moore-Penrose pseudoinverse, gradient methods, etc. When the matrix $\boldsymbol{G}$ is large, the direct inversion is practically limited by computational complexity and memory constraints and the methods referred to as row action or Algebraic Reconstruction Technique (ART) are more attractive. The main idea is that the solution is updated by successively processing each equation separately. Improvements that lead to better convergence are suggested in Simultaneous Iterative Reconstruction Technique (SIRT).

Group 2: Another group of methods try to minimize also the squared error but in the statistical sense (on average) which results in the stochastic methods based on Wiener filtering or Kalman filtering. In these methods *a priori* knowledge about the correlation structure of the solution and the noise is needed. The methods can be extended to include the correlation over space and time[13], as well.

Group 3: Depending on the specific example the notion of the *a priori* knowledge can be extended to any other useful information that is available about the field[14], e.g. the temperature is localized, the wind is a "smooth" function, etc. In many cases the information can not be incorporated into the covariance matrix and other deterministic methods like parametric estimation needs to be applied. For example, it may be known that in a certain transform domain the model parameters $\boldsymbol{m}$ have a sparse representation, i.e. $\boldsymbol{T}\boldsymbol{m} = \boldsymbol{m}_s$ where $\boldsymbol{m}_s$ is sparse. In that case, the new solution $\boldsymbol{m}_s$ to the system

$$\boldsymbol{G}\boldsymbol{T}^{\dagger}\boldsymbol{T}\boldsymbol{m} = \boldsymbol{G}\boldsymbol{T}^{\dagger}\boldsymbol{m}_s = \boldsymbol{d}$$

is searched as a minimum l_0 norm solution and it can be achieved by different algorithms as linear programming or convex projections. The concept is known as Compressed Sensing[15] and it is shown to be very useful for tomographic sampling in general[16].

In our algorithm we use a method from the first group, since at this point no a priori information is assumed. The main goal is to show that the approximation steps applied in deriving the longitudinal and the transversal components are valid and allow the reconstruction of the temperature and the wind field. Therefore, no regularization is applied and only the "pure" resolving power of the method is considered.

As the inversion step we use the conjugate gradient method with only few iterations (internal iteration of the inversion method). The choice of only a few iterations is motivated by the fact that our goal is not really to solve Eq. (13) but to converge to the solution of the non-linear problem $\boldsymbol{G}(m)\, m = \boldsymbol{d}$. While the convergence is never insured, it is always "safer" to make a smaller update $\Delta\boldsymbol{m}$ assuming that the direction of the global minimum is close to the direction of the minimum in Eq. (13).

Algorithm 1: *Non-linear tomography*

Step 1: Set the iteration $i = 0$ and $\boldsymbol{m}^i$ as an initial model (a constant or the previously best-known model)
Step 2: Compute the trajectories $\hat{\Gamma}$, matrix $\hat{\boldsymbol{G}}$ and the measurements $\hat{\boldsymbol{d}}$ for the current model $\boldsymbol{m}^i$
Step 3: Set $\Delta\boldsymbol{d} = \boldsymbol{d} - \hat{\boldsymbol{d}}$. If $\Delta\boldsymbol{d}$ is sufficiently small, stop.
Step 4: Find the corrections $\Delta\boldsymbol{m}$ as the solution of the linear system of equations[a]:

$$\hat{\boldsymbol{G}}\Delta\boldsymbol{m} = \Delta\boldsymbol{d}. \tag{13}$$

Step 5: Update the current version of the model as $\boldsymbol{m}^{i+1} = \boldsymbol{m}^i + \Delta\boldsymbol{m}$.
Step 6: Set $i = i + 1$ and go to *Step 2*.

[a]It is also possible to solve the system $\hat{\boldsymbol{G}}\boldsymbol{m}^{i+1} = \boldsymbol{d}$

Let us now concretize the reconstruction algorithm. In order to solve the problem the unknown fields have to be discretized. We define a grid encompassing the tomographic region and assume that the field can be represented by the node values assigned at the nodes and some interpolation scheme to attribute the values between the nodes. The limiting case of having infinitely many grid points is equivalent to the continuous case assuming that the underlying field is smooth.

C. Reconstruction of temperature and full wind field

In our algorithms, we use a model in which every point of an unknown parameter m inside the cells is approximated by a linear combination of the nodal values

$$m(\boldsymbol{x}) = \sum_{k=1}^{N} m_k \alpha_k(\boldsymbol{x}), \tag{14}$$

where m_k is the corresponding value at the node k, and $\alpha_k(\boldsymbol{x})$ is an interpolating function. In general, the points inside the cell are interpolated using polynomials of a certain degree. For example, one can cover the domain with a tiling of triangles, in which case $N = 3$, and the function $\alpha_k(\boldsymbol{x})$ can be the two-dimensional polynomial of order 1, i.e. the components are approximated by a plane for every triangle. This is a standard interpolation in finite element[17] methods called *linear Lagrange triangle* interpolation. The space generated by the nodal variables is the space of two-dimensional continuous piecewise linear functions. This space is convenient if the wind field is represented by its v_x and v_y components, since the continuity of the field is ensured. If the trajectories are known, Eq. (14) allows to write the set of interactions in Eqs. (8) as a linear combination of the unknown components v_x, v_y and Δc. For the longitudinal component we have:

$$\begin{aligned}
l_\Gamma &= \int_\Gamma (\Delta c\boldsymbol{n} + \boldsymbol{v})\cdot d\boldsymbol{s} = \sum_{j=1}^{J}\int_{\Gamma_j} (\Delta c\boldsymbol{n} + \boldsymbol{v})\cdot d\boldsymbol{s} \\
&= \sum_{j=1}^{J}\int_{\Gamma_j}\sum_{k=1}^{3}\alpha_k(s)(\Delta c_k\boldsymbol{n} + \boldsymbol{v}_k)\cdot d\boldsymbol{s} \\
&= \sum_{j=1}^{J}\sum_{k=1}^{3}\underbrace{\left(\int_{\Gamma_j}\alpha_k(s)\boldsymbol{n}\cdot d\boldsymbol{s}\right)}_{a_k}\Delta c_k \\
&\quad + \sum_{j=1}^{J}\sum_{k=1}^{3}\underbrace{\left(\int_{\Gamma_j}\alpha_k(s)s_x\, ds\right)}_{b_k} v_{x,k} \\
&\quad + \sum_{j=1}^{J}\sum_{k=1}^{3}\underbrace{\left(\int_{\Gamma_j}\alpha_k(s)s_y\, ds\right)}_{c_k} v_{y,k},
\end{aligned} \tag{15}$$

where the index j corresponds to the current cell, and $\Gamma_j = \Gamma \cap \text{cell}_j$. The index k denotes the vortex index within the current cell. A similar set of equations can be developed for the transversal components, by exchanging vector $\boldsymbol{s}$ with vector $\boldsymbol{s}_\perp$. In matrix notation, we can write:

$$\begin{pmatrix} \boldsymbol{G}_l \\ \boldsymbol{G}_t \end{pmatrix}\cdot\boldsymbol{m} = \begin{pmatrix} \boldsymbol{l} \\ \boldsymbol{t} \end{pmatrix}, \tag{16}$$

where $\boldsymbol{m}^T = (\boldsymbol{v}_x{}^T\ \boldsymbol{v}_y{}^T\ \Delta\boldsymbol{c}^T)$. The matrices $\boldsymbol{G}_l$ and $\boldsymbol{G}_t$ describe the linear relationship between the measurements and the unknowns, as given in (15). The equation (16) can be then solved by applying Algorithm 1.

D. Reconstruction of temperature and source-free wind field

In Sec. III.B it is shown that the longitudinal interaction allows the recovery of the temperature and 2D source-free wind field. Therefore, the system in (16) can be reduced to:

$$\boldsymbol{G}_l\cdot\boldsymbol{m} = \boldsymbol{l}.$$

In the previous case we chose to represent the wind field as $\boldsymbol{v} = [v_x, v_y]$. However, this representation does not reflect the fact that the unknown field has only a solenoidal

component. On the contrary, the representation with the potentials $\boldsymbol{\psi}$, more precisely with the derivatives of $\boldsymbol{\psi}$, i.e. $\boldsymbol{v} = \nabla\times\psi\,\boldsymbol{e}_z = [\frac{\partial\psi}{\partial y}, -\frac{\partial\psi}{\partial x}]$, discards automatically all invisible winds. However, the continuity of the wind field will be ensure if $\boldsymbol{\psi}$ but also its derivatives are continuous. Therefore, the linear Lagrange triangles are not anymore appropriate and we choose other finite element, namely the reduced *Hseih-Clogh-Tocher triangles*[18] (HCT). The HCT interpolates the third order polynomial function that is continuous together with its first order derivatives. In the HCT representation the region of interest is covered with the triangular tiles and the points inside the cells are parameterized using the value of the 3 vertex nodes m_k, and 6 directional first order derivatives $\frac{\partial m}{\partial x}$, $\frac{\partial m}{\partial y}$ (2 per node),

$$m(\boldsymbol{x}) = \sum_{k=1}^{9} m_k \alpha_k(\boldsymbol{x}).$$

This more complex tessellation adds complexity to the algorithm since now every cell is determined by 9 parameters, but the reconstructed wind is a second order polynomial function while the reconstructed temperature is a third order polynomial. The coefficients in $\boldsymbol{G}_l$ has to be computed accordingly to the new representation but similarly as before:

$$\begin{aligned} l_\Gamma &= \int_\Gamma (\Delta c\boldsymbol{n} + \nabla\times\psi\boldsymbol{e}_z)\cdot d\boldsymbol{s} \\ &= \sum_{j=1}^{J}\int_{\Gamma_j} (\Delta c\boldsymbol{n} + \nabla\times\psi\boldsymbol{e}_z)\cdot d\boldsymbol{s} \\ &= \sum_{j=1}^{J}\int_{\Gamma_j} \left(\sum_{k=1}^{9}\alpha_k(s)\,\Delta c_k\right)\boldsymbol{n}\cdot\boldsymbol{s} \\ &\quad +\nabla\times\left(\sum_{k=1}^{9}\beta_k(s)\,\psi_k\right)\boldsymbol{e}_z\cdot\boldsymbol{s}\,ds, \end{aligned}$$

where ψ_k and Δc_k are now the unknowns in the HCT model. The previous equation then needs to be incorporated in the global non-linear algorithm Algorithm 1.

V. ERROR ANALYSIS

Several technical aspects influence the performance of the tomographic reconstruction. The most important are:

1. The accuracy of the time-of-flight measurements and the angle-of-arrival/departure measurements;
2. The accuracy of the distance measurement between the transmitters and receivers;
3. The coverage of the area by sound rays (the number of emitters and receivers and their locations);
4. The resolving power of the inversion method.

Even though the accuracy depends on many factors, considering the problem as a general estimation problem helps to understand better the error. Assume that from the set of observations $\boldsymbol{d}$ the parameters $\boldsymbol{m}$ are estimated by applying an inverse mapping $\boldsymbol{G}^\dagger$ as:

$$\hat{\boldsymbol{m}} = \boldsymbol{G}^\dagger\boldsymbol{d}.$$

Taking $\boldsymbol{m}$ to be a random vector, the estimation error can be defined as $\boldsymbol{e} = \boldsymbol{m} - \hat{\boldsymbol{m}}$ and the error-error covariance matrix as

$$\begin{aligned} \boldsymbol{R}_e &= E[\boldsymbol{e}\boldsymbol{e}^T] = E[(\boldsymbol{m}-\boldsymbol{G}^\dagger\boldsymbol{d})(\boldsymbol{m}-\boldsymbol{G}^\dagger\boldsymbol{d})^T] \\ &= \underbrace{E[(\boldsymbol{m}-\boldsymbol{G}^\dagger\boldsymbol{d}_0)(\boldsymbol{m}-\boldsymbol{G}^\dagger\boldsymbol{d}_0)^T]}_{\text{mismatch}} + \underbrace{E[\boldsymbol{G}^\dagger\boldsymbol{n}_d\boldsymbol{n}_d^T\boldsymbol{G}^{\dagger T}]}_{\text{noise}}, \end{aligned}$$

where $\boldsymbol{d} = \boldsymbol{d}_0 + \boldsymbol{n}_d$, with $\boldsymbol{n}_d$ being the noise that is uncorrelated with the data and the model. The diagonal elements in $\boldsymbol{R}_e$ represent the variances of the elements in $\boldsymbol{e}$. The advantage of this analysis is that now the error can be divided into the error from the model mismatch

$$\begin{aligned} &E[(\boldsymbol{m}-\boldsymbol{G}^\dagger\boldsymbol{d}_0)(\boldsymbol{m}-\boldsymbol{G}^\dagger\boldsymbol{d}_0)^T] = \\ &\qquad \boldsymbol{R}_m - \boldsymbol{R}_{md_0}\boldsymbol{G}^{\dagger T} - \boldsymbol{G}^\dagger\boldsymbol{R}_{md_0}^T + \boldsymbol{G}^\dagger\boldsymbol{R}_{d_0}\boldsymbol{G}^{\dagger T}, \end{aligned}$$

and the error from the noise,

$$E[\boldsymbol{G}^\dagger\boldsymbol{n}_d\boldsymbol{n}_d^T\boldsymbol{G}^{\dagger T}] = \boldsymbol{G}^\dagger\boldsymbol{R}_n\boldsymbol{G}^{\dagger T}.$$

The former term vanishes when there exist a perfect model $\boldsymbol{G}$, such that $\boldsymbol{G}m = \boldsymbol{d}_0$ and $\boldsymbol{G}^\dagger\boldsymbol{G} = \boldsymbol{I}$. In reality, this is rarely the case but the gap between the model and the reality decreases as the number of transmitters and receivers and consequently the estimation resolution increases. When the model mismatch is present, this term can be evaluated if we know the correlation function of the unknown fields $\boldsymbol{R}_m$. Even though this is usually unknown, certain models for $\boldsymbol{R}_m$ can be assumed as suggested in Ref. 19. The latter term corresponds to the error in estimating the longitudinal and the transversal component. Assuming that the noise components are uncorrelated and that $\boldsymbol{n}_d^T = (\boldsymbol{n}_l^T\boldsymbol{n}_t^T)$, where $\boldsymbol{n}_l$ and $\boldsymbol{n}_t$ are the noise in the longitudinal and the transversal component respectively, we have

$$\boldsymbol{R}_n = E[\begin{pmatrix}\boldsymbol{n}_l\\ \boldsymbol{n}_t\end{pmatrix}(\boldsymbol{n}_l^T\boldsymbol{n}_t^T)] = \mathrm{diag}(\sigma_{n_l}^2,\ldots,\sigma_{n_l}^2,\sigma_{n_t}^2,\ldots,\sigma_{n_t}^2).$$

In the following, we analyze the terms $\sigma_{n_l}^2$ and $\sigma_{n_t}^2$.

A. Error in the longitudinal interaction

The error in the longitudinal component originates mostly from the time-of-flight measurements. From Eq. (5), the variance of the error in longitudinal interaction can be computed as

$$\sigma_{n_l}^2 = 2c_0^4\sigma_\tau^2,$$

assuming that both τ and τ_0 are estimated with the variance σ_τ. The Cramer-Rao lower bound for the travel

time estimates determines the lower bound for σ_τ. This bound is actually admitted when the time-of-flight is estimated from the peak of the cross-correlation between the sent and the received signal, and it amounts to be[20]:

$$\sigma_\tau^2 \geq \frac{1}{8\pi^2}\frac{1}{\mathrm{SNR}}\frac{1}{T_o B}\frac{1}{f_c^2}\frac{1}{(1+B^2/12f_c^2)}, \qquad (17)$$

where SNR is the signal-to-noise ratio, T_o observation time, f_c central frequency and B signal bandwidth. If we change the parameters in Eq. (17) with the one that we use in our experiments[21], that are $T_o = 2\ ms$, $f_c =$ 40 kHz, $B = 2$ kHz and for the two cases of SNR, we get

$$\mathrm{SNR} = 30\mathrm{dB} \longrightarrow \sigma_\tau \simeq 4.4 \cdot 10^{-8} s,$$
$$\mathrm{SNR} = 10\mathrm{dB} \longrightarrow \sigma_\tau \simeq 4.4 \cdot 10^{-7} s.$$

In the previous derivation it is assumed that τ_0 is also estimated from the time-of-flight measurements. Another possibility is to compute τ_0 from

$$\tau_0 = \frac{(\boldsymbol{x}_T - \boldsymbol{x}_R)}{c_0}. \qquad (18)$$

In this case, the error in τ_0, that originates from the error in the distance $\boldsymbol{x}_T - \boldsymbol{x}_R$, should be taken into consideration as well. Depending on the transducers type, the ambiguity in defining the center of the transmission may vary from 1mm to 50mm. This results in $\sigma_{\tau_0}^2$ that is the interval from $0.3 \cdot 10^{-8}$ to $0.7 \cdot 10^{-5}$. Moreover, there are different delays in the acquisition instruments as well as the delay in the transducers itself that will contribute to the error in $\sigma_{n_l}^2$. However, this is a systematic error that disappears when τ_0 is measured and not computed from Eq. (18).

B. Error in the transversal interaction

The variance of the error in the transversal component is going to be computed assuming that the approximation in Eq. (7) is valid. The variance then reduces to

$$\begin{aligned}\sigma_{n_t}^2 &= E[c_0^2(\cos\theta\ (y_R - y_T) - \sin\theta\ (x_R - x_T))^2] \\ &= c_0^2 E[\cos^2\theta\ (y_R - y_T)^2 - \\ &\quad 2\cos\theta\sin\theta(y_R - y_T)(x_R - x_T) + \sin^2\theta(x_R - x_T)^2] \\ &= c_0^2(\sigma_p^2\, E[\cos^2\theta] + \sigma_p^2\, E[\sin^2\theta]) \\ &= c_0^2\sigma_p^2,\end{aligned}$$

where σ_p denotes the variance of the error in the distance between the transducers. Surprisingly, σ_{n_t} does not depend on the error in the angle-of-arrival measurements, but on the other hand, σ_p^2 is always present.

After estimating $\boldsymbol{R}_n$, the complete term $\boldsymbol{G}^\dagger \boldsymbol{R}_n \boldsymbol{G}^{\dagger T}$ needs to be computed for a specific practical setup, i.e. a specific $\boldsymbol{G}^\dagger$.

VI. SIMULATION RESULTS

The simulation setup consists of a circular array that is 10 m in diameter, and it is equipped with 20 transmitters and 20 receivers. Every transmitter sends a signal to every receiver, which results in 400 transmission paths. The region of interest is covered with triangular cells of the same size. Ideally, to resolve the sound speed and the wind field at one nodal point the number of transmissions affected by that node needs to be equal or greater than the number of unknowns that characterize the node, and also the total number of transmission paths needs to be equal or greater than the total number of unknowns. However, if no a priori knowledge is considered the system of equations to be solved is usually poorly conditioned. It can be stabilized by having more measurements that the number of unknowns.

We first simulate the forward problem. Our code implements Eqs. (2) and (3) for the ray tracing in an inhomogeneous moving medium. A fifth-order Runge-Kutta algorithm is applied to integrate the ray equations forward in time. The shooting method is used to search for the correct ray. The algorithm has an adjustable integration step size and error tolerance at the receiver side. The resulting time-of-flights, the angle-of-arrivals and angles-of-departures are then taken as the measurement set. The solution is computed using the iterative algorithm described in Sec. IV, with the conjugate-gradient method as the inversion step - Step 4.

Example 2 (Perfect model match): In the first example, the perfect model match between the forward and the inverse problem is assumed and the only noise comes from the error in computing the forward model (corresponding to the tolerance error in the shooting method). In every iteration we need to solve the linearized system in Eq. (16). Figures 5(a)-(c) show the true wind field and the reconstructions for the straight ray and the bent ray model. The arrows represent the amplitude and the direction of the wind. The maximal wind speed is 5 m/s. The bent ray model achieves better result and always outperforms the straight ray model. Numerically, the root mean squared error (RMSE) of the wind reconstruction in this example was $\mathrm{RMSE}_v = 1.63$ m/s for the straight ray and $\mathrm{RMSE}_v = 1.35$ m/s for the bent ray model. The local error is usually smaller since the previous one includes the points at the border which are reconstructed with less accuracy due to the fact that less information about these points are available. The true sound speed is shown in Fig. 6(a), and the reconstruction errors for the straight and bent ray model are represented in Fig. 6(b) ($\mathrm{RMSE}_c = 2.69$ m/s) and Fig. 6(c) ($\mathrm{RMSE}_c = 0.81$ m/s) respectively. Thus, like for the wind field, the reconstruction with the bent ray model outperforms the straight ray model reconstruction. □

Example 3 (Unperfect model match and noise): In the second example, it is assumed that the 2D slice of a wind field is source-free. The measurement setup is identical to the previous one, except that in this case the region of interest is covered by the HCT triangulares. Figure 7(a) represents the true wind distribution together with the reconstructed one, with the maximal wind speed of 6.2 m/s. No difference between the true wind and the reconstructed wind can be noticed. Figure 7(b)

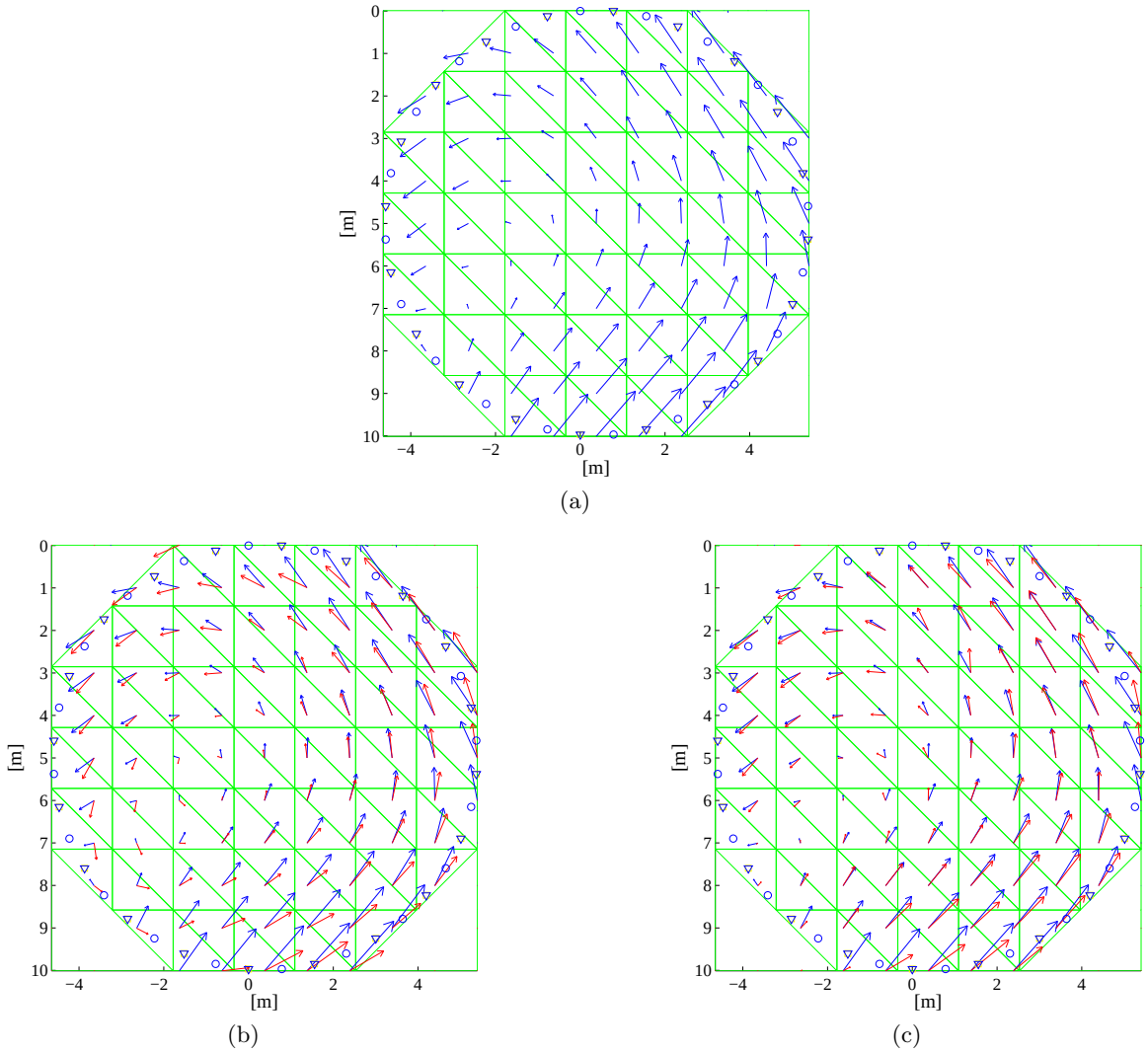

FIG. 5. Wind field: (a) True wind field; (b) Reconstructed wind field - straight ray model, $\mathrm{RMSE}_v = 1.63$ m/s; (c) Reconstructed wind field - bent ray model, $\mathrm{RMSE}_v = 1.35$ m/s.

shows the reconstruction for the noisy received signal with SNR = 10 dB. The model mismatch is created by adding 30 dB distortion to the coefficients in $\boldsymbol{G}_l$. The result shows that the reconstruction is robust to the noise and the model mismatch. The true sound speed and the corresponding reconstructions are shown in Figs. 8(a)-(c). The sound speed reconstruction is robust to the noise and the model mismatch as well. □

In summary, the simulation results show that the approximation steps applied in deriving the transversal component lead to a good reconstruction. Also, the iterative algorithms converge after 5 iterations.

VII. CONCLUSIONS

The goal of this paper was to cover important points related to the use of acoustic tomography for estimating temperature and wind in the atmosphere. It aimed in setting up properly the inverse problem and showing the techniques for obtaining the solution. Particularly, we showed that when estimating a 2D slice of temperature and wind distribution the time-of-flight measurements are not sufficient. Only the cases of source-free 2D wind fields (that are not automatically extended from a 3D source-free condition) might be faithfully reconstructed. Otherwise, a new set of measurements related to the angle-of-arrival/departure of a sound wave is needed. We also showed how these measurements can be obtained in practice. Numerical experiments confirmed that acoustic tomography offers a powerful method for studying a small scale temperature and wind distributions in the atmosphere, and stands as a good candidate to replace some of today's expensive meteorological techniques.

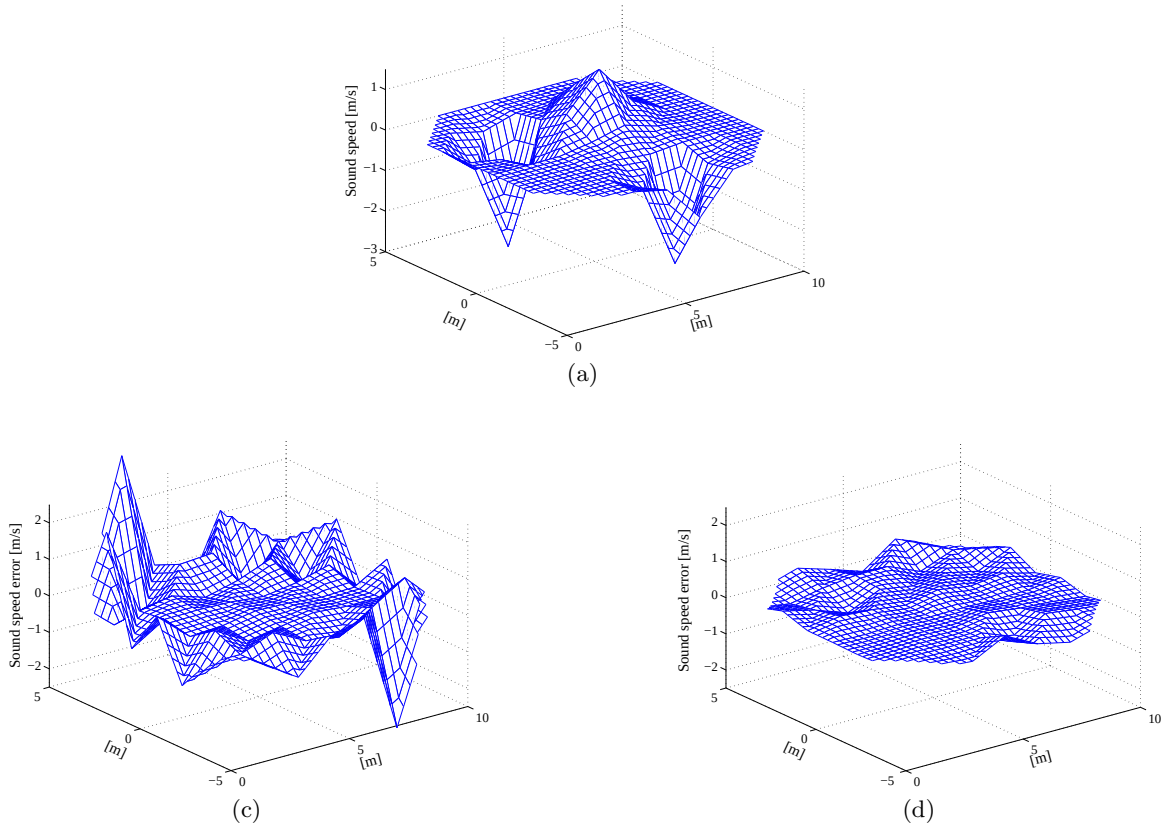

FIG. 6. Sound speed: (a) True sound speed; (b) Reconstruction error using the straight ray model, $\mathrm{RMSE}_c = 2.69$ m/s; (c) Reconstruction error using the bent ray model, $\mathrm{RMSE}_c = 0.81$ m/s.

APPENDIX: HOW TO MEASURE THE ANGLE-OF-ARRIVAL AND THE ANGLE-OF-DEPARTURE

1. Angle-of-arrival

The angle-of-arrival has to be measured precisely to guarantee an accurate estimation of the transversal component. We propose two methods. The first is based on the time difference of arrival at two positions of the test signal. The second uses the difference of amplitude of the test signal at two directional sensors placed at the same position and different orientation.

Acoustic dipole: An acoustic dipole consists of two sensors (microphones, hydrophones, etc.) placed at a certain distance on the measurement plane. If the curvature of the received sound wave can be neglected (far field assumption) the time difference of arrival of the test signal at the two sensors is proportional to the distance between the sensors and the cosine of the angle-of-arrival. Therefore, the angle-of-arrival can be estimated from this quantity and the distance between the sensors can be adjusted to obtain a certain sensitivity (this is limited by the size of the dipole).

Blumlein microphone: This method is based on the use of two directional sensors. The principle is very well known in the problem of audio stereo recording. It employs two sensors which are sensitive to acoustic pressure on a diaphragm. The pressure changes proportionally to the cosine of the angle-of-arrival, therefore the measured amplitude is related to the angle-of-arrival. If two sensors are placed approximatively at the same position forming an angle of 90 degrees on the measurement plane, the amplitude of the measured signals gives the quadrature components of the direction of arrival. In practice the sensors do not correspond perfectly to the model and a calibration procedure is required.

2. Angle-of-departure

To measure the angle-of-departure one can use an array of emitters instead of receivers, as explained in Ref. 22. The method is perfectly dual to the previous one. The first possibility is to measure the time difference of arrival between the transmitters of the array and the receiver, and deduce the angle-of-departure from this quantity. The alternative is to use the array to emit with different amplitude along different directions. The direction of departure is deduced by measuring the amplitude at the receiver for different profiles of emission. The most gen-

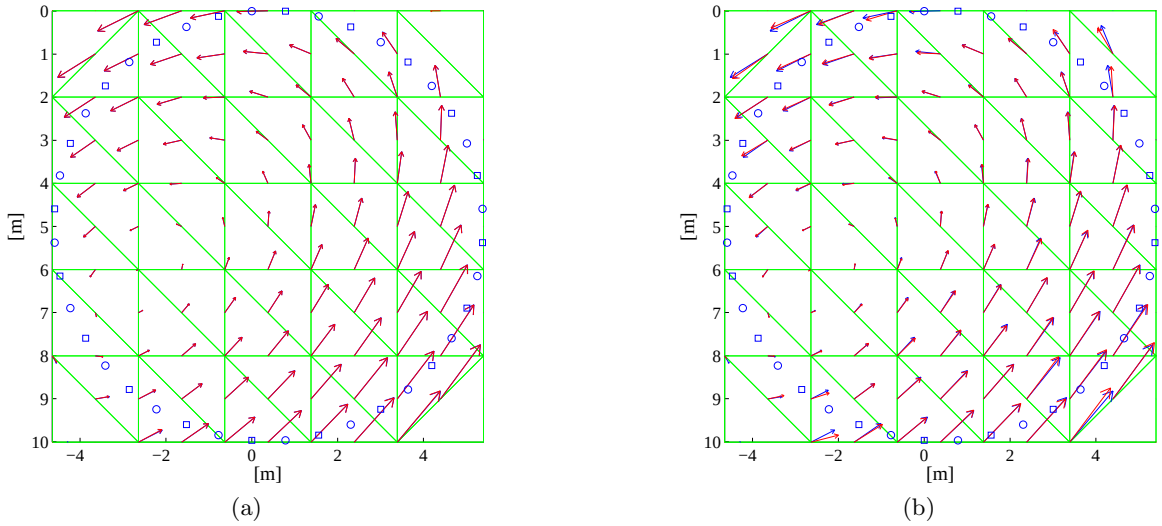

FIG. 7. Wind field: (a) The true wind field and the reconstructed wind field overlap; (b) Reconstruction error from the noisy received signal SNR = 10 dB, and for the model mismatch created by adding 30 dB of distortion to the model coefficient.

eral case is the one where arrays of transducers are used both at the emitter and the receiver. In this case both the angle of departure and arrival can be measured. This configuration is particularly convenient in cases where the same transducers can be used both for transmission and reception.

[1] J. L. Spiesberg and K. M. Fristrup, "Passive localization of calling animals and sensing of their acoustic enviroment using acoustic tomography", Am. Nat. 107–153 (1990).

[2] D. K. Wilson and D. W. Thomson, "Acoustic tomographic monitoring of the atmospheric surface layer", J. Atmos. Ocean. Tech 751–769 (1994).

[3] W. Munk and C. Wunsch, "Observing the ocean in the 1990s", Phil. Trans. R. Society London 439–464 (1982).

[4] I. P. Chunchuzov, A. I. Otrezov, I. V. Petenko, V. N. Tovchigrechko, A. I. Svertilov, A. L. Fogel, and V. E. Fridman, "Travel-time and duration fluctuation of acoustic pulses in the atmospheric boundary layer", Izvestiya, Atmospheric and Oceanic Physics (1995).

[5] A. Ziemann, K. Arnold, and A. Raabe, "Acoustic travel time tomography − a method for remote sensing of the atmospheric surface layer", Meteorology and Atmospheric Physics 43–51 (1999).

[6] S. A. Johnson, J. F. Greenleaf, C. R. Hansen, W. F. Samayoa, A. L. M. Tanaka, D. A. Christensen, and R. L. Wooley, "Reconstructing three-dimensional fluid velocity vector filds from acoustic transmission measurements", Acoustical Holography, L. W. Kessler, ed. New York: Plenum **7**, 307–326 (1977).

[7] S. J. Norton, "Unique tomographic reconstruction of vector fields using boundary data", IEEE Transactions on Image Processing **1** (1992).

[8] H. Braun and A. Hauck, "Tomographic reconstruction of vector fields", IEEE Transactions on Signal Processing **39** (1991).

[9] V. E. Ostashev, *Acoustics in moving inhomogeneous media* (E&FN SPON, London) (1997).

[10] A. Ziemann, K. Arnold, and A. Raabe, "Acoustic tomography in the atmospheric surface layer", ANN. Geophys. - Atm. Hydr. 139–148 (1999).

[11] M. Barth, K. Arnold, and A. Raabe, "Flow fiels detection using acoustic time tomography", Proceedings of the 13th Inter. Symp. for the Advancement of Boundary Layer Remote Sensing 81–82 (2006).

[12] L. Sbaiz and M. Vetterli, "Acoustic flow tomography", Technical Report, LCAV/EPFL (2003).

[13] S. N. Vercherin, V. E. Ostashev, A. Zeimann, D. K. Wilson, K. Arnold, and M. Barth, "Tomographic reconstruction of atmospheric turbulence with the use of time-dependent stochastic inversion", J. Acoust. Soc. Am. **122** (2007).

[14] I. Jovanovic, L. Sbaiz, and M. Vetterli, "Tomographic approach for parametric estimation of local diffusive sources and application to heat diffusion", in *IEEE International Conference on Image Processing* (2007).

[15] D. L. Donoho, "Compressed sensing", IEEE Trans. on Information Theory **52** (2006).

[16] I. Jovanovic, A. Hormati, L. Sbaiz, and M. Vetterli, "Efficient and Stable Acoustic Tomography Using Sparse Reconstruction Methods", in *19th International Congress on Acoustics* (2007).

[17] S. C. Brenner and L. R. Scott, *The Mathematical Theory of Finite Element Method* (Springer-Verlag New York) (2002).

[18] D. Braess, *Finite elements: Theory, fast solvers, and applications in solid mechanics* (Cambridge: University Press) (2001).

[19] D. K. Wilson, V. E. Ostashev, S. N. Vercherin, A. G. Voronovich, S. L. Collier, and J. M. Noble, "Assessment of acoustic travel-time tomography of the atmospheric surface layer", in *AMS Symposium on Boundary Layers and Turbulence* (2004).

[20] P. M. Woodward, *Probability and information theory, with applications to radar* (London : Pergamon Press) (1953).

[21] I. Jovanović, L. Sbaiz, and M. Vetterli, "Acoustic Tomography for Estimating Temperature and Wind Flow", in *13-th Intern. Symp. for the Advancement of Boundary Layer Remote Sensing* (2006).

[22] L. Sbaiz and M. Vetterli, "Tomographic methods based on direction of arrival/departure", Technical Report, LCAV/EPFL (2004).

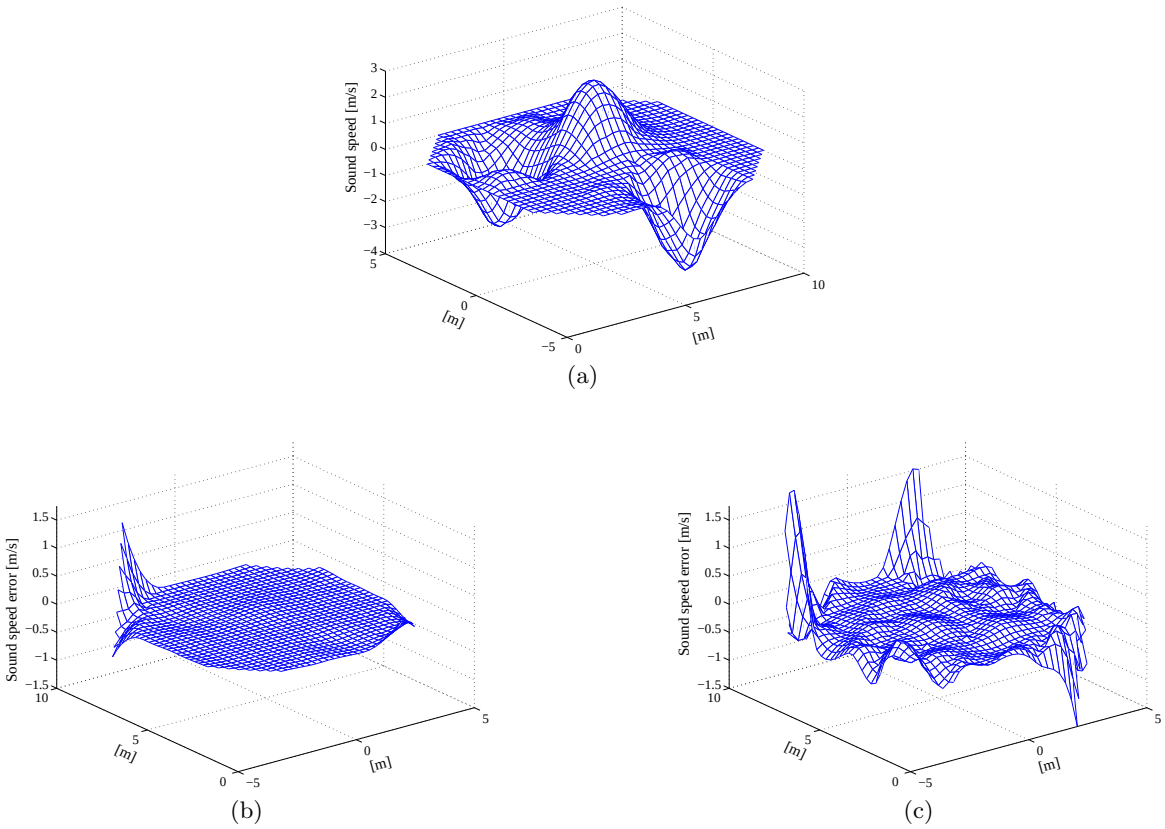

FIG. 8. Sound speed: (a) True sound speed; (b) Reconstruction error for the perfect model match; (c) Reconstruction error from the noisy received signal SNR = 10 dB and for the model mismatch created by adding 30 dB of distortion to the model coefficients.